JRIIE Journal of Research Innovation and Implications in Education
Center for Research Implications & Practice

Website:www.jriiejournal.com ISSN 2520-7504 (Online) Vol.9, Iss.2, 2025 (pp. 700 - 716)

Simulation and Design of a Grid-Connected Single-Phase Photovoltaic System Using PSCAD/EMTDC in Tanzania

Rose Sadiki Lyimo & Ally Ngulugulu
Arusha Technical College
Email: rose.sadiki1914@gmail.com

Abstract: *This study presents the simulation and design of a grid-connected single-phase photovoltaic (PV) system using PSCAD/EMTDC, specifically targeting the energy needs of Tanzania. This project explores the potential of solar energy as a sustainable solution to meet the growing energy demands in Tanzania, where energy access remains limited, with only 38% of the population having access to it. In this study, a 12-kW solar PV system was designed, incorporating MPPT controllers, DC-DC boost converters, and grid connection strategies. The simulation results show the effectiveness of the proposed system in maintaining power quality and optimising maximum power point tracking (MPPT) under varying solar irradiance and temperature conditions. The model meets international grid standards and demonstrates the feasibility of solar energy as a viable solution to the energy challenges in Tanzania.*

Keywords: *Solar Photovoltaic (PV), PSCAD/EMTDC, Maximum Power Point Tracking (MPPT), DC-DC Boost Converter, Grid-Connected System, Renewable Energy Integration, Power Quality, Tanzania Energy Sector.*

How to cite this work (APA)

Lyimo, R. S. & Ngulugulu, A. (2025). Simulation and design of a grid-connected single-phase photovoltaic system using PSCAD/EMTDC in Tanzania. *Journal of Research Innovation and Implications in Education, 9*(2), 700 – 716. **https://doi.org/10.59765/f85y9.**

1. Introduction

Energy has supported the evolution of humankind throughout history and remains an essential component of sustainable development. However, despite being indispensable, obtaining secure and sustainable energy at a minimum cost remains the biggest challenge. Traditionally, energy needs have been met by burning fossil fuels such as coal, gas, and oil. However, after being scientifically confirmed as the main source of surface global warming by the Intergovernmental Panel on Climate Change (IPCC) in 2014 (Pachauri et al., 2014), this approach is no longer viable.

Globally, such energy sources are not evenly distributed, leading to energy dependency and fluctuating energy prices (Bradshaw, 2010). A further indication of this is the rising wholesale gas prices, which are attributed to the technical and political problems faced by countries that have historically supplied Europe with energy, such as Russia.

In addition, it is important to note that fossil fuels are not replenishable and are constantly being used. Based on the remaining energy reserves and current consumption rate,(Arutyunov & Lisichkin, 2021) predicted that natural gas and crude oil will run out this century and that coal will disappear in the next century. Regardless of whether climate change is true, it is still impossible to decide what to do after the reserves run out of water.

Energy access remains a critical issue in developing countries, particularly in Africa(Brew-Hammond, 2019). Numerous African nations have been unable to fulfil the energy requirements of their populations, thereby perpetuating poverty. For instance, in Tanzania, a mere 38% of the population has access to electricity(Kichonge, 2018), with the nation predominantly relies on hydropower (36.64%) and natural gas (57.02%) for electricity generation. However, climate change has led to severe droughts, which have diminished hydropower production and resulted in power shortages, rendering the electricity system unreliable(Wasti et al., 2022).

In contrast, many renewable sources, such as wind, solar, geothermal, wave, tidal, and biomass energy, are largely untapped. With 2800 to 3500 hours of sunshine per year, Tanzania has the potential to generate 4 kWh-7 kWh/m2/day from solar energy, which exceeds Spain's solar potential("Tanzania Country Profile," 2013). Also, over 10% of its land area has a better wind potential, which is estimated to be higher than that of California (Elliott et al., 2019)

The country's electricity demand is rising due to manufacturing investments and increasing consumption (Gupta, 2020). The government plans to reform the electricity supply to attract private investment, aiming to connect 715 MW of solar photovoltaics (PV) to the national grid by 2044 (Msechu & Taylor, 2024). Solar energy's affordability (Sadat & Pearce, 2024) makes it ideal for Tanzania.

Large-scale PV systems require more land than traditional power systems (Fthenakis & Kim, 2009), making them economically challenging in Tanzania, where agriculture dominates. Additionally, implementing large-scale solar PV requires significant grid infrastructure investment, particularly in Tanzania, where power losses exceed 16.2% (Edsand & Bångens, 2024). Grid-integrated residential applications are more advantageous, minimizing transmission losses by generating power at consumption points.

Study Objectives

This study focused on these objectives:

1. To design and simulate a 12-kW grid-connected single-phase photovoltaic (PV) system using PSCAD/EMTDC, tailored to Tanzania's solar energy potential.
2. To evaluate the performance of the MPPT controller and DC-DC boost converter under varying solar irradiance and temperature conditions.
3. To assess the power quality of the system, including harmonic distortion and grid compliance, based on international standards (IEC 61000-3-2, IEEE 1547).
4. To propose modifications for upgrading the system to a three-phase configuration for future scalability.

2. Literature Review

This section discusses the literature and theoretical background of various sections of the project model. Solar photovoltaics (PV), power conversion systems, control schemes, and renewable energy grid codes were also discussed.

2.1 Solar photovoltaic

The amount of solar energy received by the Earth's surface in one hour exceeds that consumed by humans annually (Jacobson & Delucchi, 2011). Irradiance refers to the amount of energy delivered by solar radiation per square meter of the Earth's surface. This irradiance is highest at the equator and gradually decreases as the latitude angles south and north increase (Lean, 2019).

2.1.1 Solar cell generations

Solar PV modules can be used for three generations of applications. The first generation of solar cells used single-crystal and multi-crystalline Si (Kant & Singh, 2022). The second-generation category uses thin films, which are less efficient but relatively cheaper than the first generation. Third-generation solar cells are organic and have very low conversion efficiency, but are extremely cheap(Moon et al., 2019). The first generation dominates the market, but its share shrinks as the other two generations grow (El-Fayome et al., 2023; Xu et al., 2021).

2.1.2 Global solar energy trend

Solar energy has a higher installation rate than conventional power sources. Since 2000, global solar energy installations have grown by 43% annually and are expected to continue trending in several regions because of abundant resource availability, significant market potential, and cost competitiveness (International Renewable Energy Agency (IRENA), 2019). Generally, solar PV installations are growing rapidly as the cost of the technology declines significantly (Allouhi et al., 2022).

2.2 Power electronic converters

Solar PV systems require appropriate power electronic converters (PE). Solar panels typically produce direct current (DC) from 30V to 60V (Salim et al., 2023). Consequently, grid applications require voltage step-up and inversion. Stepping voltages can be achieved using either a PE DC–DC boost converter or AC transformers after the PV output voltage is inverted to AC. However, this second approach has several disadvantages, including increased cost and size and reduced system efficiency.

Transformer-less topologies are predominantly employed in grid-tied solar photovoltaic (PV) applications (Biswas et al., 2022). This methodology encompasses both two-stage power conversion (TSPC) and single-stage power conversion (SSPC). The TSPC system utilizes a boost converter to elevate a low solar PV voltage to a higher direct current (DC) output voltage, which is subsequently transformed into alternating current (AC) by an inverter. The SSPC can be implemented by connecting multiple solar panels in series prior to AC conversion or by employing a DC-to-

AC inverter with voltage boosting capabilities (Dogga & Pathak, 2019).

Both SSPC and TSPC possess distinct advantages and disadvantages. The SSPC is characterized by limited control flexibility, as modules are connected in series, thereby increasing spatial requirements and costs. Conversely, the TSPC employs DC-DC converters, offering greater flexibility and obviating the necessity for additional solar panels (Verma et al., 2022). However, the multiple conversion stages inherent in the TSPC lead to reduced efficiency due to increased losses.

2.2.1 Grid tied PV inverter topologies

There are three types of inverters: voltage source inverters (VSI), current source inverters (CSI), and impedance source inverters (ZSI). The VSI and CSI topologies are both well-known and traditional. Nevertheless, they are limited when operating with large DC variations, such as those in solar photovoltaics.

To transfer PV power to the grid, VSIs require DC voltages higher than the peak grid AC voltages. Therefore, boost converters are required to provide a higher input DC voltage. In contrast, the CSI can handle various input DC voltages. However, it requires a PV output voltage below 86.6% of the peak AC voltage for operation. Although DC-DC converters add complexity and losses to the CSI and VSI, they stabilise the DC link voltages and enable better use of the VSI/CSI. Using the ZSI, power can be transferred from a wide range of DC sources to the grid without the need for DC-DC converters. (Yuan et al., 2024). Nonetheless, this desirable behaviour is countered by the high voltage and current stresses of the system, which necessitate careful design or the use of higher-rated components that increase the cost of the system.

2.3 Maximum power point tracking (MPPT)

Solar panels are fundamentally limited to a maximum theoretical performance efficiency of 34%, which is also called the Shockley-Queisser limit (Dakua & Panda, 2023). Therefore, it is desirable to develop converters that maximise solar PV power extraction efficiency.

The output of a solar module depends on factors such as ambient temperature, solar irradiance, and sun orientation. As a result, there is only one maximum power point (MPP) for each set of operating conditions, which must be maintained at all times. (El Achouby et al., 2018). PV modules are designed to operate at maximum power through a process called maximum power point tracking (MPPT). Common MPPT algorithms include constant voltage, open-circuit voltage, short-circuit current, perturb and observe (P&O), incremental conductance (IC), and temperature methods. In addition to their differences in cost, convergence speed, sensor requirements, hardware requirements, and effectiveness, MPPT schemes differ in the complexity of their implementation. PSCAD supports only the IC and P&O methods for PV systems. The IC method automatically adjusts the operating voltage of the module without oscillations, making it the most efficient tracking method(Liu et al., 2019). Owing to its fast response time, this method is most suitable for rapidly changing weather conditions in the future. However, unlike P&O, which is easier to implement, IC is more complex and computationally challenging to implement.

2.4 Grid codes for renewable powered systems

Renewable energy sources pose challenges to grids owing to their intermittent and inverter-based nature. Grid codes are essential for ensuring a safe, secure, and economical grid. Several countries have developed renewable energy grid codes. For example, the UK grid code standard Erect G83 limits the total harmonic distortion of the current (THDi) to 3%, whereas IEC 61000-3-2 recommends a maximum of 5% (Mariscotti, 2021).

2.5 Flexibility of the Tanzania national grid

The resiliency of existing generation mixes, as well as distribution and transmission networks, determines the amount of renewable energy that can be injected into the grid or curtailed to maintain grid stability. Therefore, identifying the renewable generation uptake capacity of a grid requires an understanding of its flexibility and reliability.

Over 57.02% of Tanzania's installed capacity is fuelled by natural gas, some of which is burned in combined-cycle gas turbines (CCGTs). These generators can adapt to fluctuating renewable energy outputs, which can rapidly increase or decrease. Based on this, the grid seems ready to support small renewable power generation, which is currently supported by a feed-in tariff policy that allows a maximum of 10 MW per plant (Biririza, 2024). However, to integrate renewable power on a multimegawatt scale, more flexible generating units will need to be installed, such as CCGTs and open-cycle gas turbines (OCGTs), will need to be installed.

3. Methodology

The study utilized PSCAD/EMTDC software for modeling and simulating the PV system, including MPPT algorithms and power converters, alongside mathematical models such as the Ross model for cell temperature estimation, boost converter design equations, and SPWM modulation techniques. Key simulated hardware components included a 12 kW solar PV array, a DC-DC boost converter (100V to

500V), a single-phase H-bridge inverter (4.5 kHz switching frequency), and LC filters for harmonic mitigation. The control systems implemented the Perturb and Observe (P&O) MPPT algorithm and PI controllers for DC link voltage regulation. Real-world solar irradiance and temperature data from Shinyanga, Tanzania, were used to validate the system's performance under realistic conditions.

3.1 Solar PV Arrays Model

To design converters that can harness the maximum power from solar photovoltaic (PV) cells, it is crucial to grasp their characteristics. Therefore, an examination of solar PV principles and traits is conducted first, followed by the modelling process, which takes into account the theories discussed earlier.

3.1.1 Solar photovoltaics operating principles

The physics behind the generation of DC in solar cells, owing to solar energy, is beyond the scope of this project. However, it is important to note that a higher level of solar irradiance leads to an increased current and, therefore, power in the cell.

3.1.2 Solar cell equivalent circuit

The solar cell model is represented by a DC photo generator with a parallel diode D, which represents the charge-recombination process. Furthermore, the cell has two resistances, series and shunt, denoted by Rs and Rsh, respectively, in most cases (Kerekes et al., 2020).

3.1.3 Electrical characteristics of the solar cell

In addition to internal parameters such as Rs and Rsh, external factors such as solar irradiance and air temperature influence the electrical properties of the solar cells. Because this project is primarily concerned with solar panel power generation for power electronics interfaces, only external factors were considered in this study. Considering the critical nature of Rs, Rsh, and other internal factors in relation to solar panel efficiency, detailed information on their effects is provided in Appendix E.

According to the international standard IEC 61215, solar PV modules are rated at 1000 W/m^2 irradiance, 25˚C cell temperature, and AM 1.5 light spectrum. However, the performance of the modules varies under different conditions. Generally, as the ambient temperature increases, the open-circuit voltage decreases, which decreases the power output of the solar PV module, and vice versa. Similarly, as the solar irradiance increased, the short-circuit current increased, thereby increasing the output power.

3.1.4 Annual and Monthly solar PV temperature in Tanzania

Therefore, different operating conditions should be considered when designing solar farms. In this study, real-world temperatures and solar irradiance data from Tanzania were used. To analyse the operating temperature of the solar PV, the ambient temperature of a village in Shinyanga, located at 3.6143˚S and 33.1689°E in Tanzania, was used. The Ross model, presented in Equation 1(Ross Jr, 2021), was used to estimate the cell temperature (Tcell) from the monthly ambient temperature (Ta).

$$\mathrm{T_{cell}} = \mathrm{T_a} + \left(\frac{\mathrm{NOCT} - 20}{800}\right) * G_s$$

Where;

- G_s-Solar irradiance
- NOCT-nominal operating cell temperature of the open-circuit solar PV module at 1.0 m/s wind speed, 20°C air temperature, and 800 W/m^2 solar irradiance.

Figure 1 shows the actual annual cell and ambient temperatures. Tanzania has maximum and minimum ambient temperatures of 33°C and 14°C in October and July, respectively. These temperatures give a maximum and minimum cell temperatures of 68°C and 49°C, respectively, based on the NOCT of a typical solar panel (48 °C) (Mbawala et al., 2024) at 1000 W/m^2. From the data, the lowest cell temperature (49 °C) was chosen as the design reference because it corresponds to the highest output voltage of the solar PV model.

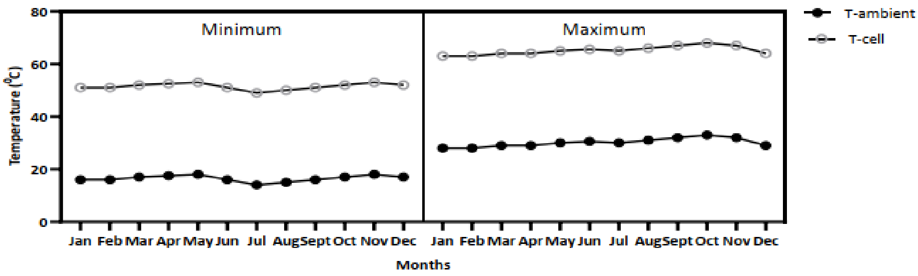

Figure 1: Annual ambient temperature and cell temperature

3.1.1 Annual hourly solar irradiance in Tanzania

In Tanzania, the peak solar irradiance is 1000 W/m^2. The data extracted from (Wasike & others, 2020) show that Tanzania's solar irradiance changes from 0 W/m^2 at 6:00 am to 1000 W/m^2 in the afternoon, and then falls back to 0 at 6:00 pm.

3.1.2 Modelling the solar PV

To design a 12 kW solar PV model, a maximum irradiance of 1000 W/m^2 and a minimum cell temperature of 49 ^{0}C were considered as the reference points. The specifications of the constructed array are presented in Table 1. As shown, more modules were connected in parallel than in series. This is because parallel-connected systems are easier to protect than series-connected systems.

Table 1:Configuration parameters of the solar PV model

Parameters	Values
Number of modules connected in series per array	2
Number of modules connected in parallel per array	25
Number of cells in series per module	92
PV cell Ideality factor	1.3
Series resistance per cell(mΩ)	20
Short circuit current in ampere (Isc) (A)	128
Open circuit voltage (Voc)	126.5
Voltage at maximum power point (Vmpp)	100
Plant rated output power (W)	12000

The PV model created based on the above specifications was simulated using PSCAD with a variable resistor. This was done to generate the Vmpp, Isc, Impp, and Voc values used in designing the next electronics converters.

3.2 DC-DC Boost converter and the switching control design

Power electronic DC-DC converters efficiently convert DC power from one voltage level to another. These converters can be categorised as buck, boost, or buck-boost converters (Mohan et al., 2003). Boost converters produce higher DC voltages from low input voltages, buck converters step down higher input DC voltages to lower output voltages, and buck-boost converters step up and down input DC voltages (Yi & Wang, 2023).

The designed solar PV system operates at a voltage lower than the DC link voltage at all times; therefore, a boost converter is the most suitable topology for this application. In addition, the power should only flow in one direction, from the solar panel to the grid; therefore, a standard boost converter is required.

3.2.1 Passive elements design and selection

The passive elements of the converter were designed based on the specifications in Table 2. The boost converter input voltage is the output voltage of the 12kW solar PV model at the maximum power point.

Table 2:Boost converter performance design specification

Parameter		Value
Input voltage	V_{in}	100V
Output voltage	V_{out}	500V
Inductor current ripples	Δi_L	≤5%
Input voltage ripples	$\frac{\Delta V_{in}}{V_{in}}$	≤1%
Output voltage ripples	$\frac{\Delta V_{out}}{V_{out}}$	≤2.5%

3.2.2 Boost converter's PWM switching

In addition to increasing the output voltage of the solar PV arrays, the DC-DC boost converter forces the modules to operate at their maximum power point and transfers that power to the DC link capacitor. According to the maximum power transfer theory, maximum power can be transferred when the source and load impedances match (Fu et al., 2021). As shown in Equation 2, the duty cycle of the boost converter (D) is varied to adjust the value of the load resistor (R_L) until it matches the solar PV resistance, that is, the point at which the maximum power is achieved.

$$R_L = 3D \text{ x } (1 - D)^2$$

As shown in Figure 2 (a), the PV output current (Ipv) and voltage (Vpv) were first low-pass filtered before being injected into the MPPT control block and set to operate with the P&O to produce the voltage corresponding to the maximum power point (Vmpp). The low-pass filter magnitude (G) and time constant (T) were set to 1 and 0.01 s, respectively.

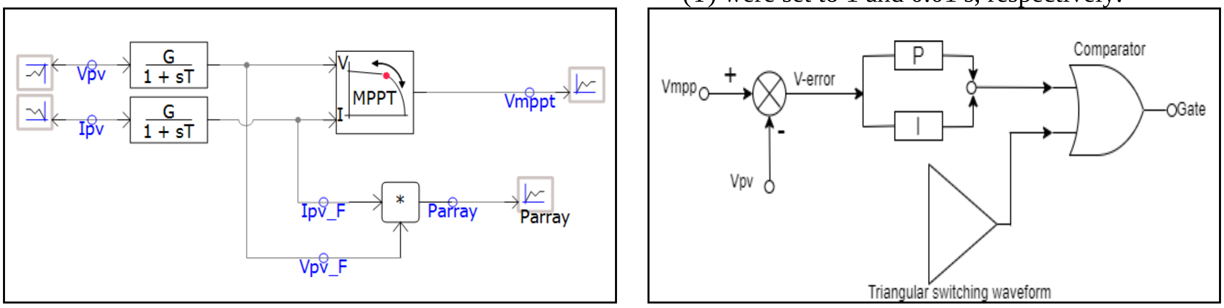

(a) (b)

Figure 2:MPPT controller model (a): MPPT block and (b): PWM switching control

As shown in Figure 2 (b), the PI controller compares Vpv and Vmpp to produce a signal that is compared with a 10kHz triangular waveform to generate a high-frequency duty cycle. Table 3 below shows the set value of the proportional and integral gain of the PI controller

Table 3: Specifications of the boost converter PI controller.

Description	Value
Proportional controller gain (Kp)	1
Integral controller gain (Ki)	0.01
Maximum controller limit set	2
Minimum controller limit set [kW]	0.0

3.2.3 Generation of the inverter modulating signals

To ensure that the inverter output conformed to IEC 61000-3-2, which specifies limits on the harmonic components of the output currents of inverter-based generators, sinusoidal pulse width modulation (SPWM) was used to generate the switching signals for the inverter. In this process, ma varies between 0 and 1, which is within the linear operating range. The inverter operating in this region prevents overmodulation, resulting in higher harmonic content in the output voltage and current (Albatran et al., 2020).

Figure 3(a) shows the inverter-modulating signal generator constructed using the PSCAD. As shown, the outputs of the reactive power control block (magnitude), the DC link voltage control block (phase-shift) explained earlier, and the frequency output variable extracted from the Fast Fourier Transform (FFT) were fed into the sine wave generator to produce a 50 Hz modulating signal wave ($V_{control}$). Using a comparator, $V_{control}$ was compared with a triangular switching signal ($V_{triangle}$), whose frequency was set to 4.5 kHz and magnitude was set between 1 and -1. The comparator was configured to generate an ON signal whenever $V_{control}$ was higher than $V_{triangle}$, and vice versa. A NOT gate was used to complement the state of the switching signals so that the two switches controlling the same leg did not receive the same switching signal at the same time, which would otherwise short-circuit the inverter legs and blow them up if they were turned ON at the same time [40]. The inverter's second-leg switching signals were generated using the same process but with a negative Vcontrol, as shown in Figure 3(b).

To avoid higher switching losses and operate outside the audible range, A switching frequency of 4.5 kHz was selected. This high switching frequency helps the low-pass filter distinguish between the fundamental frequency to maintain and the higher-order harmonic frequencies to filter out (Nauta, 2012). Furthermore, the selected switching frequency results in a frequency modulation ratio (mf) that eliminates harmonics centred at twice the switching frequency. Furthermore, the Unipolar switching mode was selected due to its ability to shift the first major harmonic from the order mf-1 to the order 2mf-1 in the inverter output (Md Haidar, 2021).

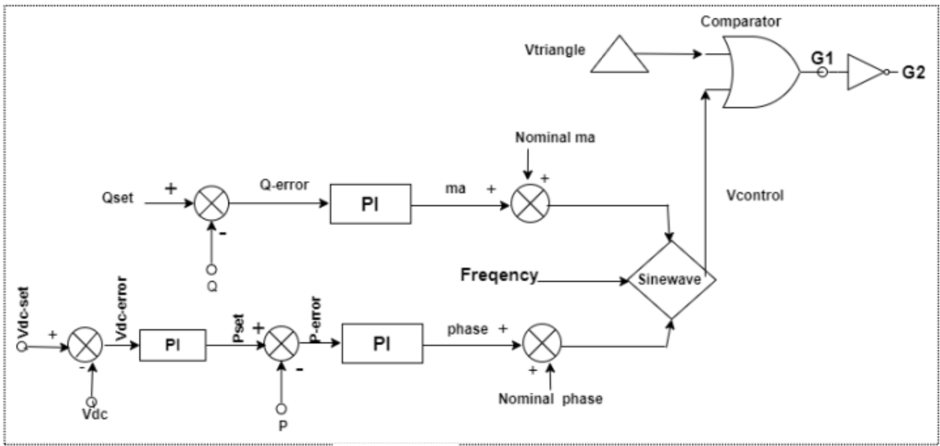

(a)

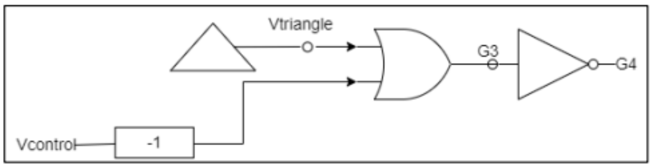

(b)

Figure 3: Inverter's SPWM modulator generator (a) signal for leg 1, (b) signal for leg 2

3.3 Utility grid model

Grid networks were represented by ideal 240V, 50 Hz AC voltage sources behind the resistive and inductive impedances representing the connecting conductors. This voltage falls under the single-phase voltage distribution network, according to Tanzania Standard 234 (Karhammar et al., 2021).

3.4 Upgrading the model to three-phase systems

Owing to anticipated load growth and electric vehicle deployment, such as that anticipated in the UK, which will reach 17.8 million by 2030 (Patil et al., 2024), the model was enhanced with a three-phase connection system. To accomplish this, various modifications were implemented in the single-phase model, as detailed in Table 4.

Table 4: Summary of changes made to the single-phase to three-phase conversion.

Descriptions	Adjusted from	Switched to	Reasons
Solar PV arrays	2 x 25	5 x 50	Increasing installed capacity
Output power[W]	12,000	120,000	
DC link voltage [V]	500	800	Avoiding overmodulation induced harmonics THD
Inverter configuration	H-bridge inverter model	Three-legged inverter model	For a three-phase network connection
Controller models	Vdc/Q control	DQ controller	

4. Results and Discussion

This section presents the simulation results of the constructed model and discusses the results obtained. The effectiveness of the model and controllers was evaluated by simulating them in the PSCAD/EMTDC environment. Simulations were conducted under various operating conditions of solar PV modules with a run duration of 10 s and a solution time step of 10 s. Figure 4 shows the designed complete single-phase model. The model has 2 × 25 solar PV modules.

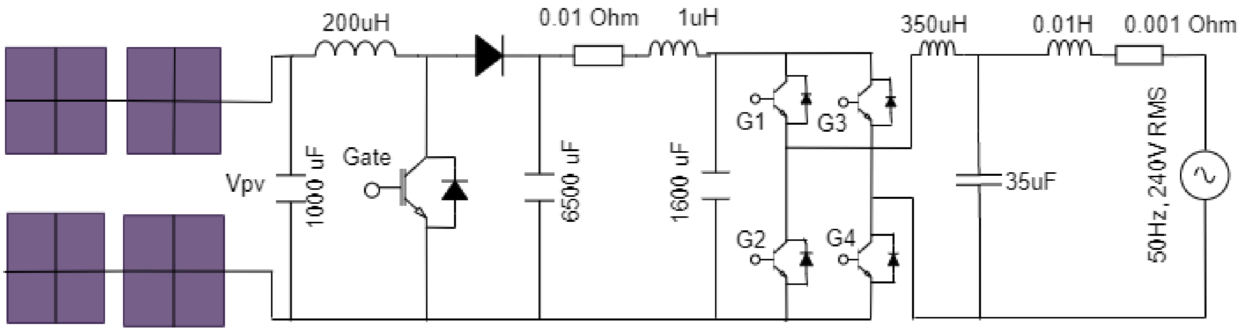

Figure 4:12kW residential solar PV system model

4.1 Operation of the DC side of the model

This section evaluates the DC side performance, including the solar PV generator, MPPT controller, and DC link.

4.1.1 Solar PV model performance

Based on the Tanzania real-world solar irradiance data (Little & Blanchard, 2022), the model was simulated at 49 °C cell temperature to observe the hourly variations of the output DC power. Figure 5 shows the generation curve of the simulated model. The maximum rated output power (i.e.,12 kW is expected in the afternoon when the solar irradiance is at its peak.

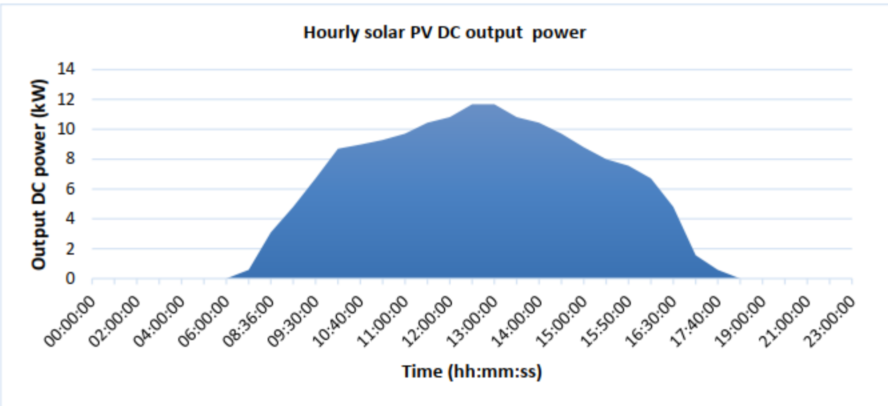

Figure 5: Expected daily generation curve measured at the solar PV terminals

4.1.2 The DC-DC converter's duty cycle

To observe the duty cycle behavior, the model was first simulated at the rated operating conditions (1000 W/m2 and 49 ℃). The simulation results shown in Figure 10a indicate that during tracking the maximum power point of the solar PV, the duty cycle oscillated to 0.85, similar to what was calculated previously, and returned to the steady state value of 0.8 once the maximum power point had been reached.

4.1.3 MPPT controller performance

In the first part of the study, a constant rated cell temperature of 49 ℃ and various solar irradiances were used to evaluate the MPPT control performance. First, the irradiance was set at 1000 W/m^2 for 3 seconds, then to 200 W/m2 for 4 seconds, and finally to 800 W/m2 for the remaining simulation time (i.e., 3 s). Figure 6b illustrates that the MPPT controller effectively identified the maximum power point of the solar PV by monitoring the voltage at which it occurred, as depicted in the VPV curve. Additionally, while fluctuations were noted during changes in irradiance, the voltage seemed to consistently hold at 100V. This suggests that the output voltage of the PV system remains relatively stable despite variations in solar irradiance.

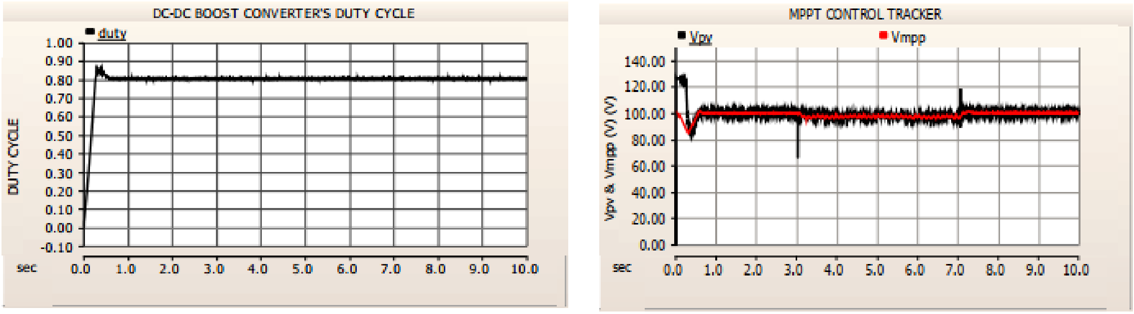

(a) (b)

Figure 6:MPPT performance evaluation (a) Duty cycle waveform at rated operating condition

In the simulation, a constant solar irradiance of 1000 W/m^2 was used to determine how temperature changes affected the MPPT performance. Thus, the model was simulated at 10°C for 3s, 40°C for 2s, 70°C for 2s, and 0°C for the remainder of the simulation (3s). Figure 11 shows the simulation results of the proposed method. Based on Figure 11a, the output voltage of the solar modules decreased and increased as the cell temperature increased and decreased, respectively. Once again, Vmpp tracked Vpv. The duty cycle varied inversely with Vpv and Vmpp, as shown in Figure 11b, which is consistent with the expected results of this study.

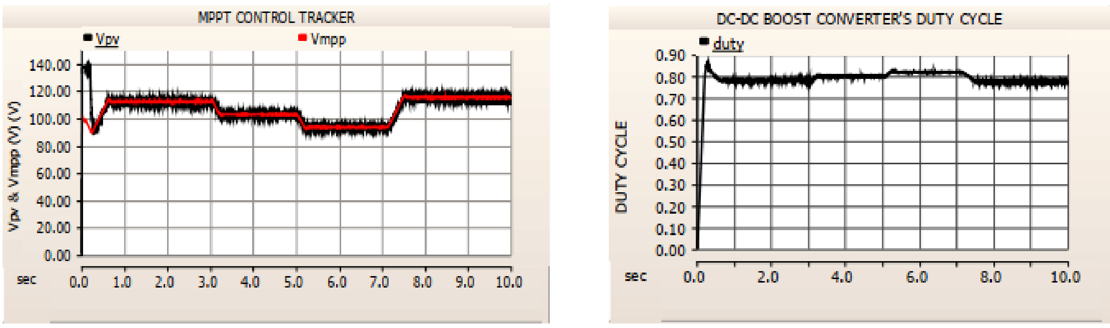

(a) (b)

Figure 7:MPPT performance (a) Variation of Vpv & Vmpp with time at different cell temperature (b) Duty cycle variations with temperature

4.1.4 The DC-link section

As part of the design criteria aimed at minimising the DCL capacitor and avoiding the cost which would have been incurred, a controller was designed and constructed to maintain the DC link voltage regardless of changes in the operating conditions. In addition, the design specification suggested 2.5% as the maximum allowable DCL voltage ripple. To verify compliance with the design specifications, the model was simulated at different solar irradiances and cell temperatures.

The simulation was first performed at 49 ℃ with irradiances set to 1000 W/m^2 for 3s, 600 W/m^2 for 3s, and then 200 W/m^2 for 4s. At a constant solar irradiance of 1000 W/m^2, the cell temperature was set to 50 °C for 4s, then 10°C for 3s, before returning to 100 °C for the remaining 3 seconds. Figure 12 shows the simulation results, which indicate that the DC link voltage remained at a constant set value of 500V despite changes in the operating conditions of the solar PV arrays. However, a few oscillations were observed when the operating conditions changed, but the controller still tracked the final set value, which justifies the successful performance of the designed DCL link voltage controller.

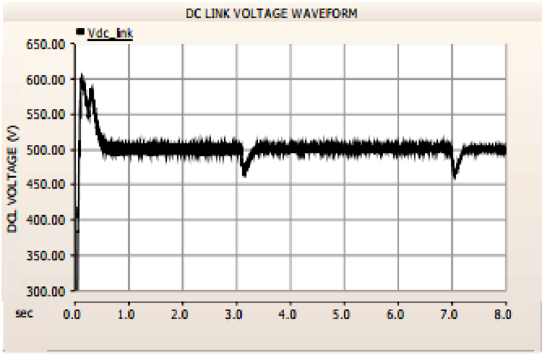

(a)

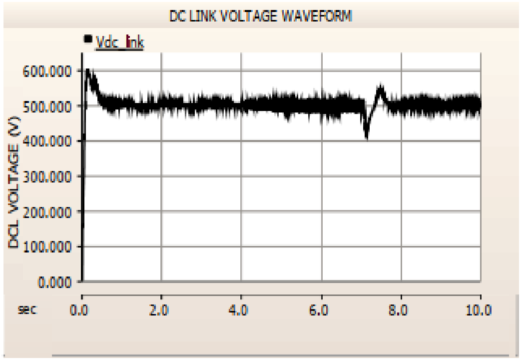

(b)

Figure 8:DC link voltage with change in operating conditions (a) Solar irradiance (b) Cell temperature

4.1.5 DCL voltage ripples

The voltage ripple was calculated as 2.9 %, which is higher than the target of 2.5%. This is probably due to the low-frequency ripples that occur more often in single-phase inverters than in three-phase inverters (Yang et al., 2023). This study showed that the operating conditions influence ripples, with higher irradiances and lower cell temperatures producing larger ripples. Because these ripples were obtained under the rated operating conditions, this value represents the maximum ripples expected in Tanzania. As part of future improvements, the appropriately sized DC capacitor will be added to the inverter's input terminals to eliminate them completely

4.2 Operation of the AC side of the model

The AC side of the constructed model, including the DC-AC inverter and LC filter, is presented and analysed in this section. The model was further tested to determine whether it met the power quality requirements imposed by the grid standards.

4.2.4 Grid connection requirements

Renewable energy grid codes have not yet been established in Tanzania, However, it is an affiliate member of the International Electrotechnical Commission (IEC), with most of its national electrotechnical standards adopting IEC and BSI standards. The requirements from the international standard IEC 61000-3-2, the UK grid code standard, Erect G83, and IEEE 1547 were used as the requirements for connecting renewable energy generation to the Tanzanian grid network.
Table 5 shows some of the grid codes imposed on inverter-based generations connection from which the quality of the power generated by the model was assessed

Table 5: General power quality requirements for inverter-based generation(Energy Network Association, 2012)

Parameter description	Agreed standard value
THD	<3%
Power factor	0.95 leading to 0.95 lagging
Grid injected current type	Sinusoidal
Grid injected voltage type	Sinusoidal
Maximum allowable DC injection	0.25% of the AC rated current

4.2.5 Inverter output voltage, current, and the LC filter

To verify that the output voltage and current of the inverter were sinusoidal as required by the grid codes, the model was simulated at its maximum output. Figure 9a shows the inverter output voltage before and after connecting the LC filter, whereas Figure 9b shows the inverter's filtered output voltage plotted with the grid network voltage. The figures show that the LC filter improved the shape of the inverter output voltage from a square wave to a sinusoidal wave that closely resembled the grid network voltage. However, the filtered inverter output voltage is not identical to the grid voltage, but this does not affect the infinite bus voltage (i.e., the grid network voltage). As shown in Figure 9c, the inverter output current waveform is sinusoidal, as required by the reference standards.

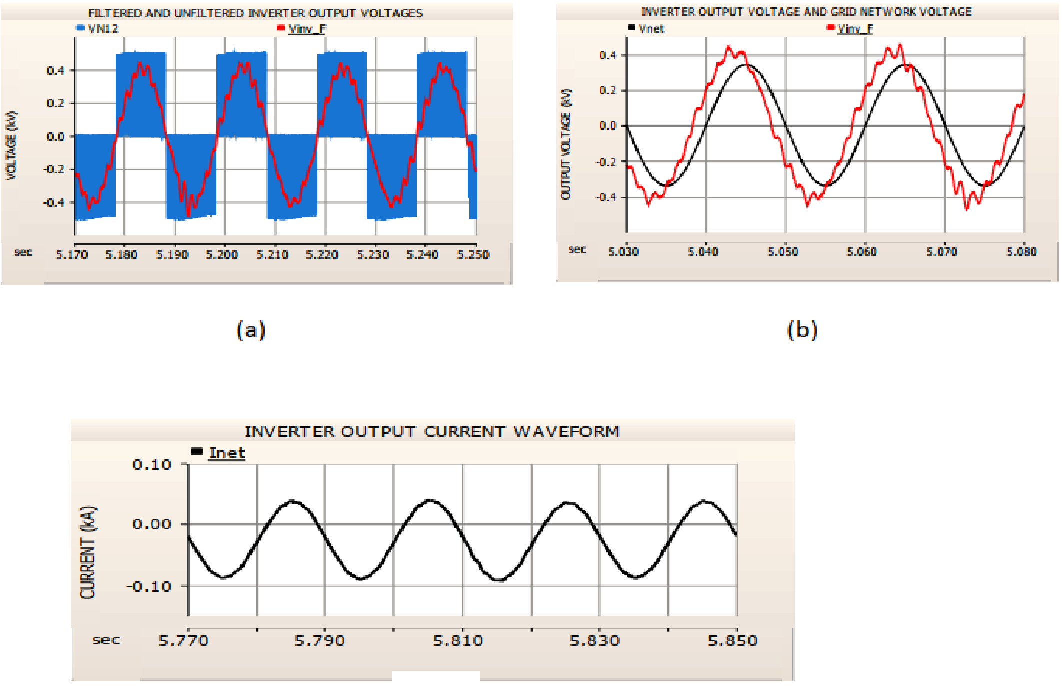

(a) (b)

(c)

Figure 9:Inverter output voltage and current waveforms (a) filtered and unfiltered voltage (Vinv_F&VN12) (b) Grid network voltage (Vnet) & Vinv_F (c) Current

4.2.6 Output active power, reactive power, and the power factor

To test the response of the output active and reactive power to the changing operating weather conditions of the system, simulations were performed at various solar irradiances and cell temperature values. At a constant cell temperature of 49˚C, the model was simulated at solar irradiances of 1000 W/m^2, 900 W/m^2, 600 W/m^{2,} and 0 W/m^2 for 2.5s each. Additionally, the solar irradiance was fixed at 1000 W/m^2, and the simulations were run at 100°C, 68°C, 49°C, and 25°C for 2.5s each. Figure 14 shows the simulation results of the proposed method. As displayed in (a) and (b), the output active power increased with a reduction in the cell temperature and decreased with a reduction in solar irradiance. This demonstrates the model's effectiveness, as expected, as explained in the literature review.

Even so, the Figures show that the active and reactive powers initially oscillated before reaching a steady state. This situation may have been caused by the MPPT controller oscillating for about 0.5seconds during tracking the maximum power point. The reactive power was set to 0 kVA at all simulation times.

Following the simulation at the rated operating conditions, plots of the output DC power (Pgen) and grid-injected power (Pgrid) were produced, along with the voltage and current waveforms. It is evident from Figure 10 (c) that the inverter output current and voltage are nearly in phase, demonstrating the model's compliance with the power factor requirement. According to Figure 10 (d), Pgen and Pgrid are 11.8 kW and 10.8 kW, respectively, in the steady state. In other words, the efficiency of the designed converter was 91.5%, which indicates that it was slightly resistive. However, this efficiency is not that terrible when compared to an actual system studied in (Yang et al., 2023), which provided 89.83% efficiency despite being a single-stage power conversion system.

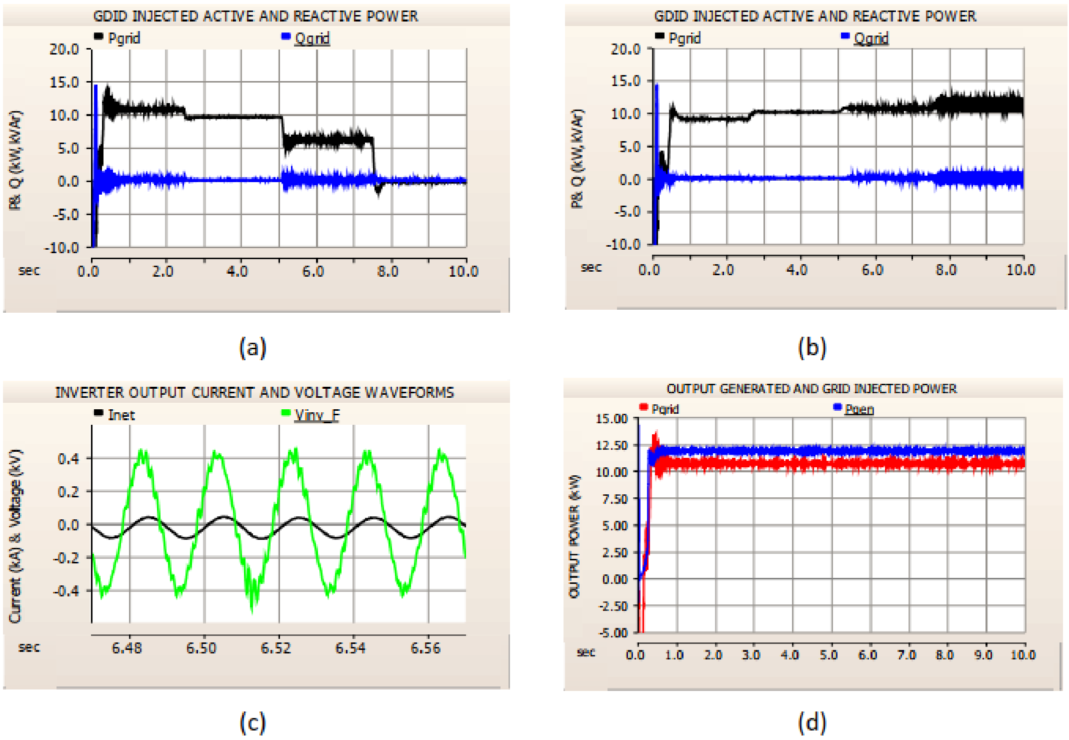

Figure 10:Output active power response to change in (a) solar irradiance (b) ambient temperature (c) inverter output current and voltage waveforms (d)Output Pgrid and Pgen

4.2.7 Total Harmonic Distortion Analysis

To avoid damaging other utility-connected equipment, PV systems must have low harmonic distortion levels. Because the grid network system voltage is robust, only the inverter output current was studied because of the minimal impact of voltage harmonics. The PSCAD model used to measure the harmonic distortion in percentage is shown in Figure 11.

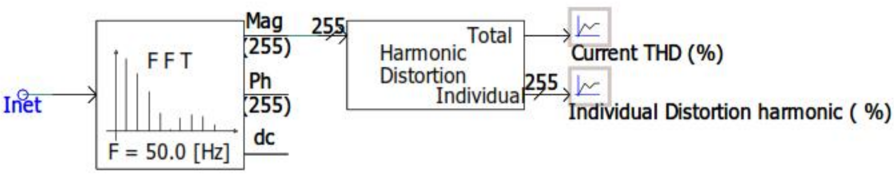

Figure 11:Current harmonic measurement block

From Figure 11, the Fast Fourier Transform (FFT) block was used to calculate the harmonic magnitude of the inverter output current connected to its input. The FFT output was connected to the input terminals of the harmonic magnitude block to generate the total and individual harmonic distortions. The FFT block was configured to output 255 harmonics, with a fundamental frequency set to 50 Hz.

To examine the power quality, the model was simulated under the rated operating condition, and the individual current harmonics were recorded. As shown in Table 6, when compared to the individualized harmonics and THD, no resulting current harmonic distortion was found to violate the recommended values.

Table 6: Inverter’s rated current harmonic distortion

Harmonic number (h)	Measured harmonic (%)	Recommended harmonics (%) [55]

3	0.19	<2.3
5	0.32	<1.14
7	0.18	<0.77
9	0.10	<0.40
11	0.04	<0.30
13	0.08	<0.21
THDi	1.78	<3

4.2.8 Effects of changes in operating conditions on output power quality

Analyses were conducted to assess the output current quality under different solar irradiance conditions. The model was simulated with varying solar irradiances, and the current THD was recorded. As shown in Figure 12, THDi decreased with increasing solar irradiance. This implies that PV systems operating at low irradiances inject more harmonics into the grid. As a result, it might be necessary for solar PV system operators to either improve harmonic filtering methods or disconnect their PV systems from the grid at lower irradiance levels to avoid paying huge penalties for over-harmonic operation.

Although lower irradiances result in more harmonics in the output current, the THDi observed in this model's simulation at low irradiances was too high and not as expected. Poor passive elements were likely selected, leading to the higher DC offsets observed at lower irradiances. Because it is unlikely that Tanzania will ever have much variation in ambient temperature due to its proximity to the equator, the effects of temperature variations on the quality of the output current were not studied.

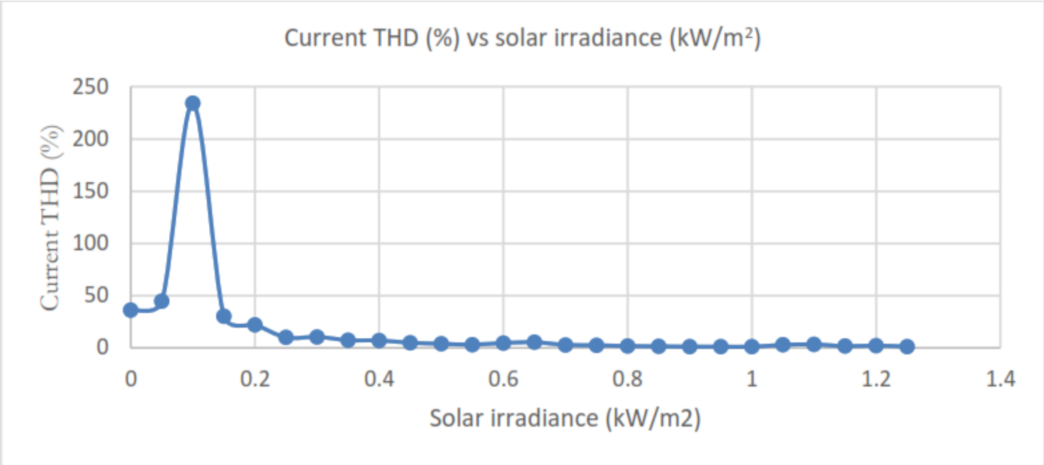

Figure 12: Variation of the current THD with solar irradiance

4.2.9 Daily hourly grid injected active power

Using the irradiance data from Tanzania, the model was simulated to generate the expected daily grid-injected power. The simulation results shown in Figure 13 indicates that the maximum power is injected during the afternoon when the solar irradiance is the highest.

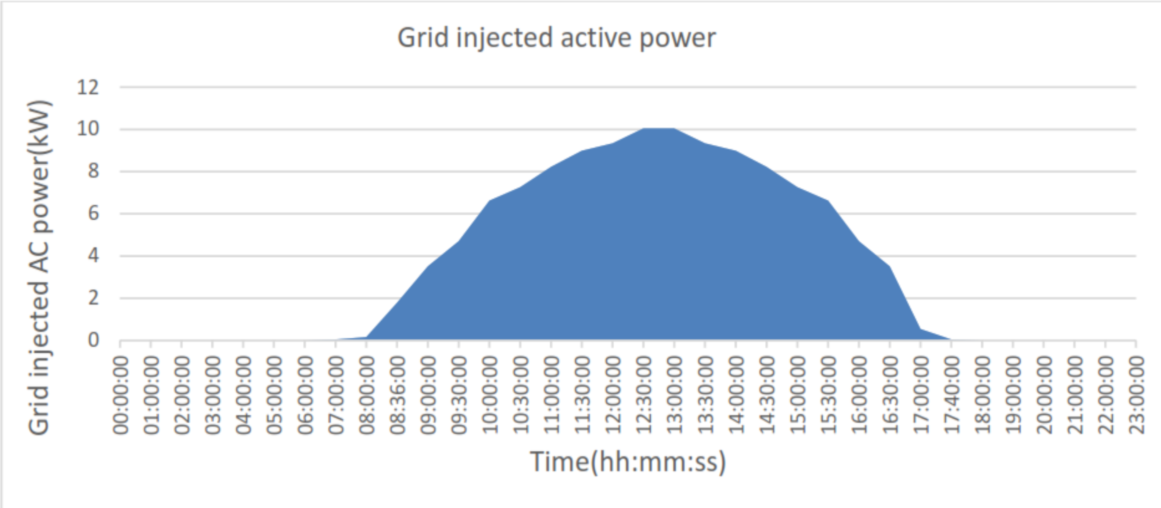

Figure 13: Daily output AC power injected into the grid network

5. Conclusion and Recommendations

5.1Conclusions

This project involved the design and development of a 12 kW single-phase solar PV PSCAD model. The model was based on the TSPC system, with the selection of passive elements being mathematically justified. Based on the simulation results, the model represented the expected results as the operating conditions changed. Furthermore, despite changes in the operating conditions, the model maintained a power factor close to unity and maintained an acceptable power quality level, as specified in IEC 61000-3-2, IEEE 1547, and UK grid code G 83. The performance of the inverter controller was verified and found to be adequate. In addition, the effectiveness of the MPPT controller under rapidly changing weather conditions was demonstrated, as were the power flow and DC link voltage control strategies.

Nevertheless, the model has unexpected shortcomings, such as overshooting the THDi at low irradiances and not maintaining the DC link voltage ripples within the design limits.

5.2 Recommendation

The design included a detailed battery storage system model for off-grid applications as one of the objectives. Unfortunately, time constraints prevented the achievement of this objective. However, in Tanzania, where most people live off-grid, battery storage systems are essential to this model. Thus, it will be included in future work.

Moreover, a detailed study is required to identify an MPPT control method with a reduced delay compared to the time taken by the method used in this model to achieve the MPP. In addition, passive elements will be redesigned in the future to bring the DC link voltage ripples within a targeted range. For the overshooting of the THDi at lower irradiances, further studies are needed to establish a harmonic filtering technique that can provide better results or determine the minimum irradiance at which the solar PV model must be disconnected from the grid. However, disconnections would mean losing free energy, which is not a good option for the system.

References

Albatran, S., Allabadi, A. S., Al Khalaileh, A. R., & Fu, Y. (2020). Improving the performance of a two-level voltage source inverter in the overmodulation region using adaptive optimal third harmonic injection pulsewidth modulation schemes. *IEEE Transactions on Power Electronics*, *36*(1), 1092–1103.

Allouhi, A., Rehman, S., Buker, M. S., & Said, Z. (2022). Up-to-date literature review on Solar PV systems: Technology progress, market status and R\&D. *Journal of Cleaner Production*, *362*, 132339.

Arutyunov, V. S., & Lisichkin, G. V. (2021). Energy resources of the 21st century: problems and forecasts. Can renewable energy sources replace fossil fuels. *Russian Chemical Reviews*, *86*(8), 777.

Biririza, E. G. M. (2024). Energy Transition Agenda in Tanzania Within the Auspice of Sub-Saharan Africa: A Review of the Power Sector. *International Journal of Economy, Energy and Environment*, *9*(3), 59–76.

Biswas, M., Biswas, S. P., Islam, M. R., Rahman, M. A., Muttaqi, K. M., & Muyeen, S. M. (2022). A new transformer-less single-phase photovoltaic inverter to improve the performance of grid-connected solar photovoltaic systems. *Energies*, *15*(22), 8398.

Bradshaw, M. J. (2010). Global energy dilemmas: a geographical perspective. *Geographical Journal*, *176*(4), 275–290.

Brew-Hammond, A. (2019). Energy access in Africa: Challenges ahead. *Energy Policy*, *38*(5), 2291–2301.

Dakua, P. K., & Panda, D. K. (2023). Analysis of various hole transport layers (HTLs) on the performance of CZTS-solar cell. *Physica Scripta*, *98*(3), 35110.

Dogga, R., & Pathak, M. K. (2019). Recent trends in solar PV inverter topologies. *Solar Energy*, *183*, 57–73.

Edsand, H.-E., & Bångens, L. (2024). Power struggles: Advances and roadblocks of solar powered mini grids in Tanzania. *Energy Reports*, *11*, 342–354.

El-Fayome, E., Abdelhamed, M. A., El-Shazly, A., Abouelatta, M., & Zekry, A. (2023). End Of Life Management Of Solar Panels. In *National Radio Science Conference, NRSC, Proceedings* (Vols. 2023-May). https://doi.org/10.1109/NRSC58893.2023.10152958

El Achouby, H., Zaimi, M., Ibral, A., & Assaid, E. M. (2018). New analytical approach for modelling effects of temperature and irradiance on physical parameters of photovoltaic solar module. *Energy Conversion and Management*, *177*, 258–271.

Elliott, D. L., Wendell, L. L., & Gower, G. L. (2019). *An assessment of the available windy land area and wind energy potential in the contiguous United States*.

Energy Network Association. (2012). *Engineering Recommendation G83 Issue 2*. *2*(2).

Fthenakis, V., & Kim, H. C. (2009). Land use and electricity generation: A life-cycle analysis. *Renewable and Sustainable Energy Reviews*, *13*(6–7), 1465–1474.

Fu, M., Zhang, T., Ma, C., & Zhu, X. (2021). Efficiency and optimal loads analysis for multiple-receiver wireless power transfer systems. *IEEE Transactions on Microwave Theory and Techniques*, *63*(3), 801–812.

Gupta, V. (2020). A case study on economic development of Tanzania. *Journal of the International Academy for Case Studies*, *26*(1), 1–16.

International Renewable Energy Agency (IRENA). (2019). Future of solar photovoltaic: Deployment, investment, technology, grid integration and socio-economic aspects. In *Irena: Vol. November*. https://www.irena.org/-/media/Files/IRENA/Agency/Publication/2019/Oct/IRENA_Future_of_wind_2019.pdf

Jacobson, M. Z., & Delucchi, M. A. (2011). Providing all global energy with wind, water, and solar power, Part I: Technologies, energy resources, quantities and areas of infrastructure, and materials. *Energy Policy*, *39*(3), 1154–1169.

Kant, N., & Singh, P. (2022). Review of next generation photovoltaic solar cell technology and comparative materialistic development. *Materials Today: Proceedings*, *56*, 3460–3470.

Karhammar, R., Sanghvi, A., Fernstrom, E., Aissa, M., Arthur, J., Tulloch, J., Davies, I., Bergman, S., & Mathur, S. (2021). Sub-saharan africa: Introducing low-cost methods in electricity distribution networks. *ESMAP Technical Paper*, *104*(06).

Kerekes, T., Teodorescu, R., & Borup, U. (2020). Transformerless photovoltaic inverters connected to the grid. *APEC 07-Twenty-Second Annual IEEE Applied Power Electronics Conference and Exposition*, 1733–1737.

Kichonge, B. (2018). The status and future prospects of hydropower for sustainable water and energy development in Tanzania. *Journal of Renewable Energy*, *2018*(1), 6570358.

Lean, J. L. (2019). Cycles and trends in solar irradiance and climate. *Wiley Interdisciplinary Reviews: Climate Change*, *1*(1), 111–122.

Little, M., & Blanchard, R. (2022). Pre-feasibility methodology to compare productive uses of energy supplied by stand-alone solar photovoltaic systems: A Tanzanian case study. *Energy for Sustainable Development*, *70*, 497–510.

Liu, T., Wong, T. T. Y., & Shen, Z. J. (2019). A survey on switching oscillations in power converters. *IEEE Journal of Emerging and Selected Topics in Power Electronics*, *8*(1), 893–908.

Mariscotti, A. (2021). Power quality phenomena, standards, and proposed metrics for dc grids. *Energies*, *14*(20), 6453.

Mbawala, J. R., Li, H., Ndabagenga, D. M., Zeng, J., & Mlonganile, P. N. (2024). Assessment of the Spatio-Temporal Trends of Annual Extreme Temperature Indices over Tanzania during the Period of 1982-2022. *Journal of Geoscience and Environment Protection*, *12*(1), 33–50.

Md Haidar, I. (2021). *A PI based coordinated maximum power point tracking controller for grid connected photovoltaic system/Md Haidar Islam*. Universiti Malaya.

Mohan, N., Undeland, T. M., & Robbins, W. P. (2003).

Power electronics: converters, applications, and design. John wiley \& sons.

Moon, M. M. A., Rahman, M. F., Hossain, J., & Ismail, A. B. M. (2019). Comparative study of the second generation a-Si: H, CdTe, and CIGS thin-film solar cells. *Advanced Materials Research*, *1154*, 102–111.

Msechu, A. S., & Taylor, R. S. (2024). Macroeconomic Determinants of Renewable Energy Consumption in Tanzania: A Time Series Analysis from 1990-2020. *Tanzanian Economic Review*, *14*(1), 18–44.

Nauta, B. (2012). *Analog CMOS filters for very high frequencies* (Vol. 190). Springer Science \& Business Media.

Pachauri, R. K., Allen, M. R., Barros, V. R., Broome, J., Cramer, W., Christ, R., Church, J. A., Clarke, L., Dahe, Q., Dasgupta, P., & others. (2014). *Climate change 2014: synthesis report. Contribution of Working Groups I, II and III to the fifth assessment report of the Intergovernmental Panel on Climate Change*. Ipcc.

Patil, G., Pode, G., Diouf, B., & Pode, R. (2024). Sustainable Decarbonization of Road Transport: Policies, Current Status, and Challenges of Electric Vehicles. *Sustainability*, *16*(18), 8058.

Ross Jr, R. G. (2021). Flat-plate photovoltaic array design optimization. *14th Photovoltaic Specialists Conference*, 1126–1132.

Sadat, S. A., & Pearce, J. M. (2024). The threat of economic grid defection in the US with solar photovoltaic, battery and generator hybrid systems. *Solar Energy*, *282*, 112910.

Salim, M. B., Sari, T. N., Suseno, N., & Rajabiah, N. (2023). The Effect of Using Monocrystalline Solar Panels on Alternating Current (AC) and Direct Current (DC) Lamps. *International Journal of Research and Review*, *10*(7), 274–282.

Tanzania country profile. (2013). *Trade in the East African Community: Facilitation Measures and Potential Benefits*, 155–171.

Verma, P., Sharma, A. K., Pandey, V. S., & Noor, A. (2022). TSPC-HNTL: True Single Phase Clock technique for High speed, Noise Tolerance, and Low power. *Analog Integrated Circuits and Signal Processing*, *112*(2), 333–345.

Wasike, W. W., & others. (2020). *Assessment of the solar radiation potential of the Thika-Nairobi area, panel sizing and costing*.

Wasti, A., Ray, P., Wi, S., Folch, C., Ubierna, M., & Karki, P. (2022). Climate change and the hydropower sector: A global review. *Wiley Interdisciplinary Reviews: Climate Change*, *13*(2), e757.

Xu, Y., Li, J., Tan, Q., Peters, A. L., & Yang, C. (2021). Global status of recycling waste solar panels: A review. *Waste Management*, *75*, 450–458.

Yang, P., Xu, S., Meng, F., Zhang, Z., Zhou, R., & Xu, J. (2023). A low frequency ripple current suppression strategy for single-phase photovoltaic grid-connected inverter. *IEEE Journal on Emerging and Selected Topics in Circuits and Systems*, *13*(2), 536–544.

Yi, F., & Wang, F. (2023). Review of voltage-bucking/boosting techniques, topologies, and applications. *Energies*, *16*(2), 842.

Yuan, J., Liu, P., Siwakoti, Y. P., & Blaabjerg, F. (2024). Z-source converters and their classifications. In *Control of Power Electronic Converters and Systems: Volume 4* (pp. 3–25). Elsevier.